Fracture of Zircaloy-4 fuel cladding tubes with hydride blisters

Vincent Macdonald, David Le Boulch, Arthur Hellouin de Menibus, Jacques Besson, Quentin Auzoux, Jérôme Crépin, Thomas Le Jolu

Available online at www.sciencedirect.com

ScienceDirect

Procedia Materials Science 3 (2014) 233 – 238

Procedia Materials Science

www.elsevier.com/locate/procedia

20th European Conference on Fracture (ECF20)

Fracture of Zircaloy-4 fuel cladding tubes with hydride blisters

Vincent Macdonald[a,b*], David Le Boulch[a], Arthur Hellouin de Menibus[a], Jacques Besson[b], Quentin Auzoux[a], Jérôme Crépin[b], Thomas Le Jolu[a]

[a]*CEA, DEN, 91191 Gif Sur Yvette, France*
[b]*MinesParistech, 10 rue Henri-Auguste Desbruères, 91100 Corbeil-Essonne, France*

Abstract

The influence of hydride blister on cold worked stress relieved Zircaloy-4 cladding tubes fracture toughness at room temperature was studied using hoop tensile tests and plane strain tensile tests. The experimental macroscopic fracture stress and strain values and an elastic-plastic finite element analysis of the mechanical tests with the CAST3M code were used to calculate the J-integral and estimate the fracture toughness for several blister depths from 120 to 240 µm.

Selection and peer-review under responsibility of the Norwegian University of Science and Technology (NTNU), Department of Structural Engineering

Keywords: Zircaloy-4, fuel cladding, hydride blister, fracture toughness.

1. Introduction

This study is focused on the fracture behavior of cold worked stress relieved (CWSR) Zircaloy-4 (Zy-4), a zirconium alloy used in pressurized water reactors (PWR) as fuel cladding tubes. These tubes are oxidized during operation in the reactor by the water coolant. Thus, an oxide layer (zirconia) grows at the water-metal interface and hydrogen ingresses into the cladding.

The zirconia is brittle and may be locally spalled off if it grows up to a very high thickness. The induced thermal gradient in the cladding triggers hydrogen thermo-diffusion toward the coldest area, where the oxide was spalled off. Beyond the solubility limit of hydrogen in zirconium, the diffusing hydrogen atoms precipitate into zirconium hydrides at this cold spot, to form a highly hydrided area called hydride blister.

* Corresponding author. *E-mail address:* vincent.macdonald@cea.fr

Selection and peer-review under responsibility of the Norwegian University of Science and Technology (NTNU), Department of Structural Engineering
doi:10.1016/j.mspro.2014.06.041

It was demonstrated by Papin et al. (2007) that hydride blisters reduce the fuel cladding ductility and can cause its failure under hypothetic accidental conditions. Through-thickness crack propagation and fracture toughness of hydrided zirconium alloys was previously analyzed at 25°C, 300°C, 375°C by Dubey et al. (1999), Kuroda et al. (2000), Pierron et al. (2003), Glendening et al. (2004), Desquines et al. (2005), Bertolino et al. (2006), Tomiyasu et al. (2007), Daum et al. (2007), Georgenthum et al. (2008), Udagawa et al. (2009), Sartoris et al. (2010), Hsu et al. (2011), Raynaud et al. (2012). It appears in these studies that hydrogen content and hydride orientation are key parameters to assess zirconium alloys fracture toughness at room temperature.

In the present study, the effect of hydride blisters on the cladding fracture resistance was evaluated by performing hoop tensile tests (HT) and plane strain tensile tests (PST) on unirradiated Zy-4 rings containing artificially grown hydride blisters of various depths, at room temperature. Experimental results and calculations of J-integral by finite element method are discussed in order to evaluate the influence of hydride blister on Zircaloy-4 cladding tubes fracture toughness at room temperature.

2. Experimental study

The studied material was a commercial cold worked stress relieved (CWSR) Zy-4 fuel cladding tube, with a thickness of 570 μm and a diameter of 9.5 mm, provided by CEZUS. Its chemical weight composition was 1.3% Sn, 0.21% Fe, 0.11%Cr, 0.13% O, Zr balance. Some cladding tubes were pre-hydrided at 300 wppm by gaseous charging, and hydride blisters were grown on these samples by a cold spot technique developed by Hellouin de Menibus et al. (2013). This technique consisted in applying a thermal gradient on the tube to trigger hydrogen diffusion towards this cold spot, to generate a hydride blister at this location. Due to the lower density of δ-hydrides compared to the zirconium, the blister grew with a protrusion on the tube external diameter, as shown in Fig. 1.

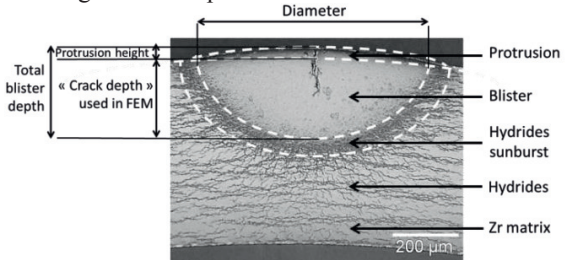

Fig. 1. Metallography of a hydride blister grown on a Zy-4 tube, radial-circumferential plane, Hellouin de Menibus (2013).

The protrusion of the hydride blister was measured by a non-destructive optical method of shadowscopy. In Hellouin de Menibus et al. (2013), a correlation between the height of the protrusion and the blister total depth measured by metallography was determined. A mean ratio of protrusion to blister total depth of 22 % was obtained so that it was possible to estimate the blister total depth by measuring the protrusion height.

Some samples were then machined into hoop tensile (HT) and plane strain tensile (PST) specimens, see Fig. 2. Stress biaxiality ratios (σ_{zz} / $\sigma_{\theta\theta}$) are approximately 0 and 0.5 for HT and PST mechanical tests respectively, according to Desquines et al. (2011). Specimens containing hydride blisters were machined with the blister located at the center of the gage section. These mechanical tests were carried out on both non-hydrided and hydrided specimens containing a hydride blister or not. Among these tests, two HT tests and six PST tests were performed on hydrided Zy-4 rings containing a hydride blister. Two 8.30 mm diameter D-shaped mandrels were used on an INSTRON servo-hydraulic tensile machine, with a 50 kN load cell (accuracy in load measurement is better than 0.5%), at an approximate strain rate along the loading direction of 10^{-1} s^{-1}, at room temperature. No lubricant was used between the sample and the mandrels.

The engineering stress-strain curves obtained during the tensile tests are shown in Fig. 3. The presence of hydride blister led to a macroscopic brittle behavior which became more pronounced all the more the blister depth increased.

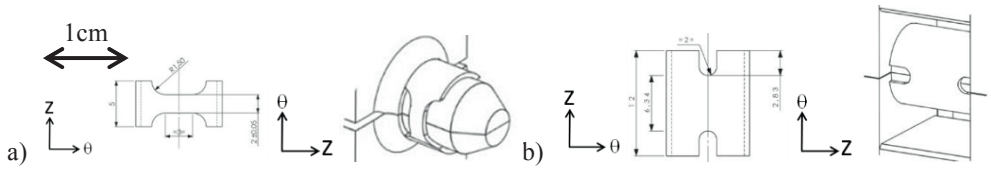

Fig. 2. a) HT specimens b) PST specimens (Le Saux et al. 2010).

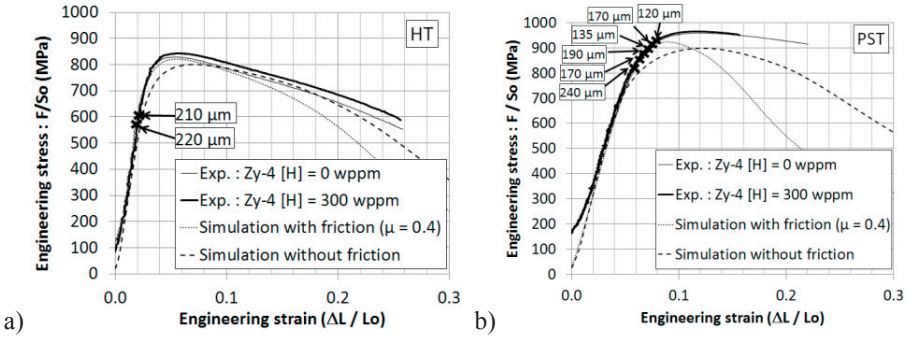

Fig. 3. Engineering stress-strain curves for non-hydrided and hydrided (a) HT tests (b) PST tests, containing blisters or not. Crosses indicate the failure of samples containing a blister, blister depths are given in the boxes.

Fracture surfaces were examined by scanning electron microscope (SEM) and blister total depths were checked (Fig. 4). The uncertainty on the blister depth measurement by SEM was evaluated to be <7%. The obtained mean ratio of blister protrusion height to total blister depth was 22 ± 2%, in accordance with the previously established correlation. Differences between estimated depths and depths measured by SEM are <10%. The mean ratio of blister total depth to the blister half diameter was 72 ± 3%. In accordance with Le Saux et al. (2010) results, non-hydrided samples and homogenously hydrided samples failed by ductile fracture according to the dimples shown on fracture surfaces, important necking and final shear fracture. Secondary cracks perpendicular to the loading direction and corresponding to broken hydrides are observed in homogenously hydrided samples. Samples containing blisters failed in a brittle manner. Cracks initiated in the blister propagated in a radial-axial plane normal to the principal circumferential stress. Therefore, Elastic-Plastic Fracture Mechanics seemed to be an appropriate tool to model this type of blister induced embrittlement.

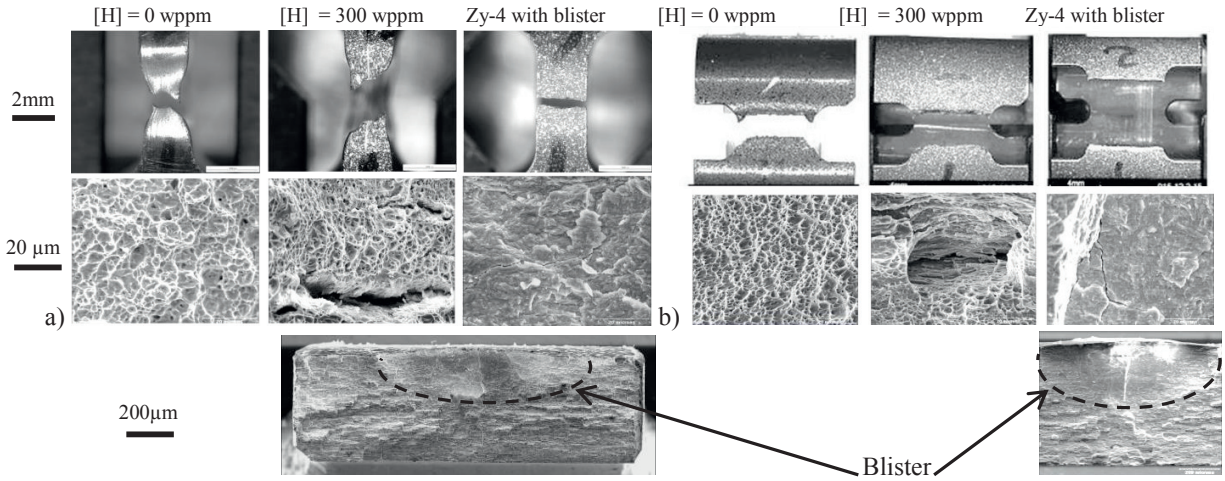

Fig. 4. Fracture profiles (first row) and fracture surfaces (following rows) of non-hydrided Zy-4, homogeneously hydrided Zy-4, and Zy-4 with blister for (a) HT tests; (b) PST tests.

3. Numerical Analysis

Calculations were carried out with the finite element code CAST3M, developed by CEA (http://www-cast3m.cea.fr/), for the HT and PST samples. The material was assumed to be isotropic, and calculations were performed with elastic and elastic-plastic models with isotropic hardening, on one eighth of the sample regarding load and geometry symmetries, although there is a blister on only one gage section. This approach should be considered as a first modeling step as the material effective behavior is anisotropic and elastic-viscoplastic, as detailed in Le Saux et al. (2008).

The elastic-plastic model was determined on un-cracked non-hydrided HT geometry, and used for the computations of HT and PST samples containing blisters. The comparison between experimental and simulated engineering stress versus engineering strain is respectively shown for HT and PST geometry in Fig. 3a) and Fig. 3b), with and without friction between sample and mandrel, using a Coulomb friction coefficient of $\mu = 0.4$, as suggested by Le Saux et al. (2008). On those figures, the experimental stiffness was adjusted so that it fits the simulated one in order to correct the displacement measure from the tensile machine compliance. The friction coefficient value modifies the macroscopic mechanical stress-strain curves of the samples. This elastic-plastic model, determined on HT geometry, seemed to be less suitable when applied to PST geometry, according to Fig. 3. It appears to under-estimate stresses and to allow more plasticity for the material. The observed differences could be due to the fact that material anisotropy and viscoplasticity are not taken into account in these calculations. As a first approach, a contact without friction was used in the following calculations.

It was demonstrated in Desquines (2005) that blisters have an elastic-brittle behavior. Consequently, they were modelled in the present analysis by a semi-elliptical radial-axial surface crack on the center of the gage length, which was meshed using the FIS_3D procedure implemented in CAST3M, as shown in Fig. 5. Mesh size at the crack tip was between 5 and 10 µm, depending on blister depth. It was assumed that the blister of a certain total depth measured by SEM is equivalent to a single crack of the same initial depth minus the protrusion height, as shown in Fig.1. As a first approximation, the blister volume was assumed to have the same mechanical properties as the Zy-4.

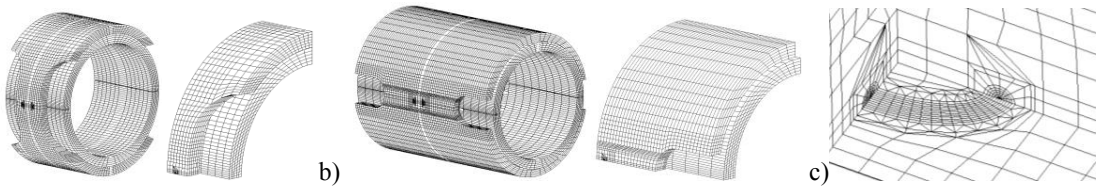

Fig. 5 Meshes of a) HT and b) PST samples, containing c) a semi-elliptical surface crack on the center of the gage length.

The J-integral calculations, based on the work of Rice et al. (1968), are commonly used to predict crack propagation. J-integral curves were determined for several blisters depths corresponding to experimental tests, using the G-theta method implemented in CAST3M. This G-theta method consists in virtually disturbing the crack and calculating the corresponding energy variation, over a given path that surrounds the crack tip, as described by Suo and Combescure (1992). J_{Ic} values corresponding to the measured failure stresses and strains were picked up and can be converted into fracture toughness K_{Ic} values, according to Eq. (1). Under plane stress (HT) and plane strain (PST) conditions, J_{Ic} can be respectively expressed by:

$$J_{Ic} = \frac{K_{Ic}^2}{E} \qquad J_{Ic} = \frac{(1-\nu^2)\, K_{Ic}^2}{E} \qquad (1)$$

where K_{Ic} is the material fracture toughness, E the Young modulus, and ν the Poisson ratio.

The hypotheses of confined plasticity at the crack tip and J-integral path independence were studied. The plasticity area was located up to 20 µm from the crack tip, so that plasticity is well confined as the sample thickness is 570 µm. J-integral path independence was evaluated for different paths away from 20 to 50 µm from the crack tip. Differences between J_{Ic} values for the smallest and largest paths were estimated at +3% for the largest paths.

J-integral curves for HT samples containing blisters obtained with an elastic model and an elastic-plastic model with a failure stress and a failure strain analysis are respectively shown in Fig. 6a) and Fig. 6b). It appeared that plasticity was to be taken into account. Critical J-integral values for HT samples containing blisters obtained by both failure stress and strain analysis were similar.

J-integral curves for PST samples containing blisters obtained with an elastic-plastic model with a failure stress and a failure strain analysis are respectively shown in Fig. 6c) and Fig. 6d). Critical J-integral values for PST samples are higher and more scattered when determined by a failure stress analysis than by a failure strain analysis, this is due to the elastic-plastic model which allowed too much plasticity for the material, as seen in Fig. 3b).

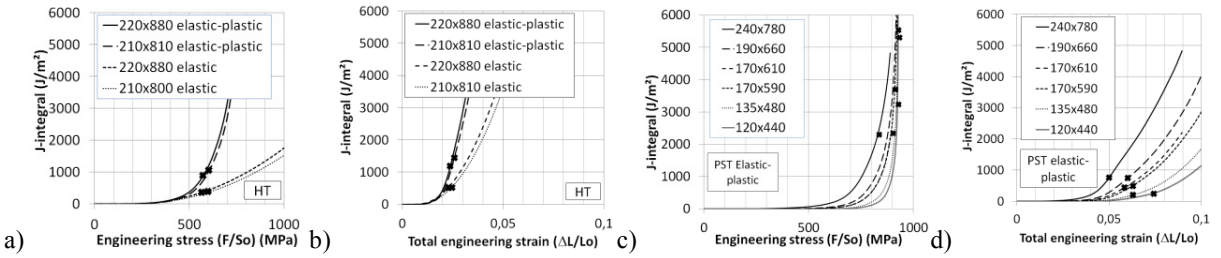

Fig. 6 J-integral curves for a) HT – stress analysis b) HT - strain analysis c) PST - stress analysis d) PST - strain analysis; samples containing several sizes of blisters : crack depth x diameter. Crosses indicate the failures.

Using Eq. (1) with E = 95 GPa and $\nu = 0.342$, fracture toughness K_{Ic} values corresponding to critical J-integral J_{Ic} values obtained with the elastic-plastic model were estimated between 10 and 12 MPa.m$^{1/2}$ for HT simulations and between 5 and 24 MPa.m$^{1/2}$ for PST simulations. Fig. 7) shows the dependence of calculated fracture toughness K_{Ic} with the total blister depth minus protrusion height. As expected, the K_{Ic} estimated on PST samples were higher and more scattered following the failure stress analysis than following the strain analysis.

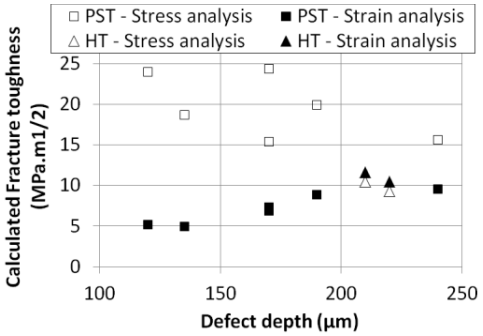

Fig. 7 Fracture toughness K_{Ic} versus defect size, calculated with an elastic-plastic model for HT and PST samples, with stress and strain analysis

Crack length and fracture toughness might have been under-estimated by the procedure presented here because the radial hydrides composing the "sunburst" around the blister (see Fig. 1) were not taken into account, whereas they may extend the brittle zone. Sunburst lengths were measured for eight blisters on pictures obtained by optical microscopy, and were estimated from 30 to 60 µm, depending on blister depth. Moreover, it was demonstrated by Hellouin de Menibus (2013) that hydrogen content in the substrate beneath the blister is not homogeneous and can be more than 1000 wppm, whereas samples were homogeneously pre-hydrided at about 300 wppm before applying the cold spot to generate a blister. Considering these two remarks, the results presented here compare well with the results from the open literature detailed in the following paragraph.

Zy-4 fracture toughness values are not necessarily the same between axial and radial directions. According to the Electric Power Reasearch Institute EPRI report (2001), irradiated Zy-4 materials showed fracture toughness values at room temperature of 12 to 15 $MPa.m^{1/2}$ for hydrogen contents of about 1000 wppm. Raynaud et al. (2012) estimated normal fracture toughness at 25°C of CWSR hydrided Zy-4 sheets from 45 to 10-15 $MPa.m^{1/2}$, when increasing hydrogen content from 0 to 500 wppm and radial hydrides fraction from 0 to 90%.

4. Conclusions

Hoop tensile tests and plane strain tensile tests were performed at room temperature on CWSR Zy-4 rings containing hydride blisters or not. The blister induced embrittlement was observed. A finite element analysis was carried out using an elastic-plastic model. Blisters were simulated by a semi-elliptical surface crack in the radial-axial plane, and J-integral values were determined to evaluate the material fracture toughness.

In the future, several modifications of the modeling should improve the accuracy of the fracture toughness estimation presented here. Firstly, the constitutive equations should take into account the material anisotropy and viscosity. Secondly, friction should be considered in calculations of samples containing a blister as it was done in the other calculations. Finally, the crack depth equivalent to a given blister depth has to be better estimated, by taking into account the hydrides sunburst.

References

Bertolino, G., 2006, Influence of the crack-tip hydride concentration on the fracture toughness of Zircaloy-4, Journal of Nuclear Materials, vol. 348, pp 205-212.

Daum, R., 2007, Mechanical behavior of high burnup Zircaloy-4 fuel cladding - experiments and analyses of ring compression loading, 15th International Symposium on Zirconium in the Nuclear Industry. Sunriver, Oregon, United States.

Desquines, J., 2005, Mechanical properties of Zircaloy-4 PWR fuel cladding with burnup 54-64MWd/kgU and implications for RIA behavior, 14th International Symposium on Zirconium in the Nuclear Industry, ASTM STP 1467. Stockholm, Sweden.

Desquines, J., 2011, The issue of stress state during mechanical tests to assess cladding performance during a reactivity-initiated accident (RIA), Journal of Nuclear Materials, vol. 412 issue 2, pp 250-267.

Dubey, J.S., Assessment of hydrogen embrittlement of Zircaloy-2 pressure tubes using unloading compliance and load normalization techniques for determining J-R curves, Journal of Nuclear Materials, vol. 264, pp20-28.

Electric Power Research Institute EPRI report, 2001, Fracture toughness data for zirconium alloys.

Georgenthum, V., 2008, Fracture mechanics approach for failure mode analysis in CABRI and NSRR tests, International Topical Meeting on Light Water Reactor Fuel Performance. Seoul, Korea.

Glendening, A., 2004, Failure of hydrided Zircaloy-4 under equal biaxial and plane-strain tensile deformation, Journal of ASTM international, vol. 2 issue 6, pp 833-850.

Hellouin de Menibus, A., 2013, Formation and Characterization of Hydride Blisters in Zircaloy-4 Cladding Tubes, accepted by Journal of Nuclear Materials.

Hsu, H., 2011, Effect of hydride orientation on fracture toughness of Zircaloy-4 cladding, Journal of Nuclear Materials, vol. 408, pp 67-72.

Kuroda, M., 2000, Influence of precipitated hydride on the fracture behavior of Zircaloy fuel cladding tube, Journal of Nuclear Science and Technology, vol. 37 issue 8, pp 670-675.

Le Saux, M., 2008, A model to describe the anisotropic viscoplastic mechanical behavior of fresh and irradiated Zircaloy-4 fuel claddings under RIA loading conditions, Journal of Nuclear Materials, vol. 378 issue 1, pp 60-69.

Le Saux, M., 2010, Behavior and failure of uniformly hydrided Zircaloy-4 fuel claddings between 25°C and 480°C under various stress states, including RIA loading conditions, Engineering Failure Analysis vol. 17 issue 3, pp 683-700.

Papin, J., 2007, Summary and interpretation of the CABRI REP-Na program, Nuclear Technology, vol. 157 issue 3, pp230-250.

Pierron, O.N., 2003, The influence of hydride blisters on the fracture of Zircaloy-4, Journal of nuclear materials 322, pp 21-35.

Raynaud, P., 2012, Crack growth in the through-thickness direction of hydrided thin-wall Zircaloy sheet, Journal of nuclear materials, vol. 420 issue 1-3, pp 69-82.

Sartoris, C., 2010, A consistent approach to assess safety criteria for reactivity initiated accidents, Nuclear Engineering and Design, vol. 240 issue 1 pp 57-70

Suo and Combescure, 1992, On the application of G-theta method and its comparison with De Lorenzi's approach, Nuclear Engineering and Design, vol. 135, pp207-224.

Tomiyasu, K., 2007, Influence of cladding-peripheral hydride on mechanical fuel failure under reactivity-initiated accident conditions, Journal of Nuclear Science and Technology, vol. 44 issue 5, pp 733-742.

Udagawa, Y., 2009, Stress intensity factor at the tip of cladding incipient crack in RIA-simulating experiments for high burnup PWR fuels, Journal of Nuclear Science and Technology, vol. 46 issue 10, pp 1012-1021.